

Multiphoton Microscopy of Prostate and Periprostatic Neural Tissue: A Promising Imaging Technique for Improving Nerve-Sparing Prostatectomy

Rajiv Yadav, M.D., M.Ch.,^{1,*} Sushmita Mukherjee, Ph.D.,^{2,*} Michael Hermen, M.D.,¹ Gerald Tan, M.D.,¹ Frederick R. Maxfield, Ph.D.,² Watt W. Webb, Sc.D.,³ and Ashutosh K. Tewari, M.D., M.Ch.¹

Abstract

Background and Purpose: Various imaging modalities are under investigation for real-time tissue imaging of periprostatic nerves with the idea of improving the results of nerve-sparing radical prostatectomy. We explored multiphoton microscopy (MPM) for real-time tissue imaging of the prostate and periprostatic neural tissue in a male Sprague-Dawley rat model. The unique advantage of this technique is the acquisition of high-resolution images without necessitating any extrinsic labeling agent and with minimal phototoxic effect on tissue.

Materials and Methods: The prostate and cavernous nerves were surgically excised from male Sprague-Dawley rats. The imaging was carried out using intrinsic fluorescence and scattering properties of the tissues without any exogenous dye or contrast agent. A custom-built MPM, consisting of an Olympus BX61WI upright frame and a modified MRC 1024 scanhead, was used. A femtosecond pulsed titanium/sapphire laser at 780-nm wavelength was used to excite the tissue; laser power under the objective was modulated via a Pockels cell. Second harmonic generation (SHG) signals were collected at 390 (± 35 nm), and broadband autofluorescence was collected at 380 to 530 nm. The images obtained from SHG and from tissue fluorescence were then merged and color coded during postprocessing for better appreciation of details. The corresponding tissues were subjected to hematoxylin and eosin staining for histologic confirmation of the structures.

Results: High-resolution images of the prostate capsule, underlying acini, and individual cells outlining the glands were obtained at varying magnifications. MPM images of adipose tissue and the neural tissues were also obtained. Histologic confirmation and correlation of the prostate gland, fat, cavernous nerve, and major pelvic ganglion validated the findings of MPM.

Conclusion: Real-time imaging and microscopic resolution of prostate and periprostatic neural tissue using MPM is feasible without the need for any extrinsic labeling agents. Integration of this imaging modality with operative technique has the potential to improve the precision of nerve-sparing prostatectomy.

Introduction

RADICAL PROSTATECTOMY (RP) for organ-confined prostate cancer is an effective method of treatment but can result in erectile dysfunction in a significant proportion of patients. Although the development of nerve-sparing anatomic retropubic RP has made it possible to reduce the likelihood of postoperative impotence, there is still room for improvement.

The reported rates of postoperative potency after nerve-sparing RP range from 21% to 86%.^{1–5} One of the important reasons for the variability in results between different centers

is related to the inability of surgeons to identify and preserve the cavernous nerve in a reliable and consistent manner. It is usually impossible to see the cavernous nerve with the naked eye or even with laparoscopic magnification. The location of the nerves is often assumed by the surgeon on the basis of the anatomic description of the pelvic plexus and neurovascular bundle.⁶ Another contributory factor is the individual variation in the course of the cavernous nerves and their relationship to the prostate and urethra.^{7–9}

Thus, improved visualization of the periprostatic nerves is expected not only to lead to improved results of nerve-sparing RP, but also to help in individualized preservation of nerves.

¹Department of Urology and Urologic Oncology Outcomes and ²Department of Biochemistry, Weill Medical College of Cornell University, New York, New York.

³School of Applied & Engineering Physics, Cornell University, Ithaca, New York.

*These authors contributed equally to this work.

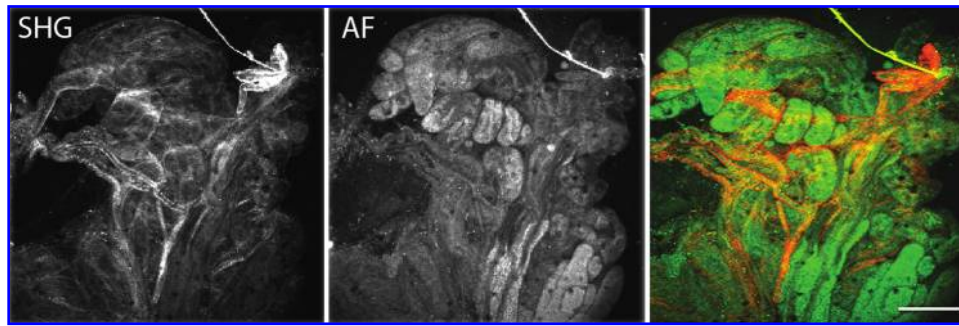


FIG. 1. Multiphoton microscopy of rat prostate at low magnification (4 \times). A single optical section from the middle of the tissue is shown. The colored image is the processed composite of second harmonic generation (SHG) signal and autofluorescence (AF) from the prostatic tissue. Seen are the outlines of autofluorescent acini composed of prostatic cells (green) and SHG signal from the fibrous stroma around the acini (red). Scale bar: 500 μm .

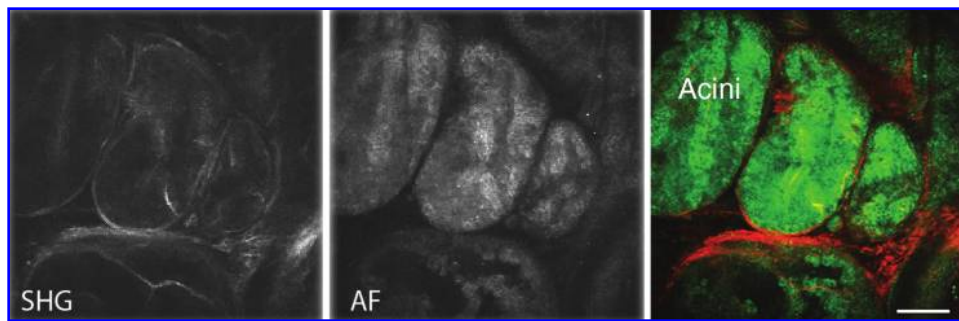


FIG. 2. Multiphoton microscopy of prostate using a 20 \times objective showing individual acini surrounded by the fibromuscular stroma. The colored image is the processed composite of second harmonic generation (SHG) signal (left) and autofluorescence (AF) (middle) from the prostatic tissue.

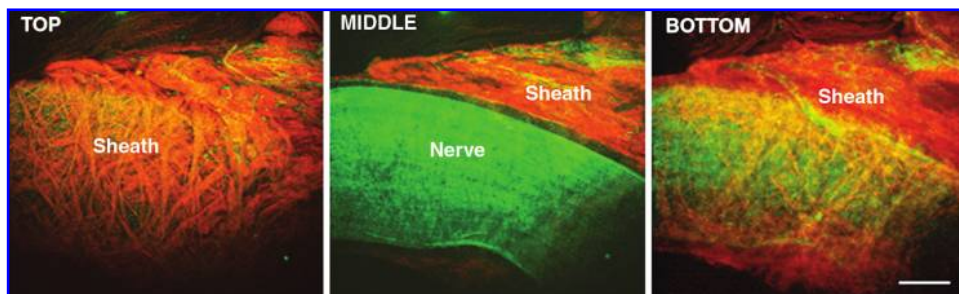


FIG. 3. High magnification (20 \times) multiphoton microscopy image of rat femoral nerve. Seen are the second harmonic generation signal from the fibrocollagenous sheath (red) and autofluorescence (green) from the nerve, presumably coming from the axoplasm and the cytoplasm of Schwann cells. Note how the sheath wraps around the nerve bundle. Scale bar: 100 μm .

In this study, we investigated the use of multiphoton microscopy (MPM) as a novel bioimaging modality for real-time prostatic and periprostatic tissue visualization.

Materials and Methods

Our experimental design included the imaging of nerves and prostate from freshly euthanized male Sprague-Dawley rats through a protocol approved by the Institutional Animal Care and Use Committee. Rats were chosen because of ease of handling and our thorough familiarity with their genitourinary anatomy, including the nerves in relation to the prostate. The rat cavernous nerve model is a well-recognized model for radical RP-associated neurogenic erectile dysfunction.^{10,11} The prostate, cavernous nerve, major pelvic ganglion, blad-

der, and seminal vesicles were identified after a midline celiotomy incision in 10 male Sprague-Dawley rats weighing 300 to 600 g.

A stepwise approach for imaging, identification, correlation, and confirmation of neural tissue was followed. The first step involved the *ex vivo* imaging of a large known peripheral nerve. The first set of experiments served to familiarize us with the exact identification of neural tissue in a reliable and consistent manner. The second step involved the imaging of the cavernous nerve, prostate capsule, and underlying acini along with the periprostatic tissues. In the final step, the cavernous nerve, major pelvic ganglion, fat, vessels, prostate, and periprostatic tissues were first imaged by MPM and subsequently subjected to histologic confirmation by hematoxylin and eosin (H&E) staining.

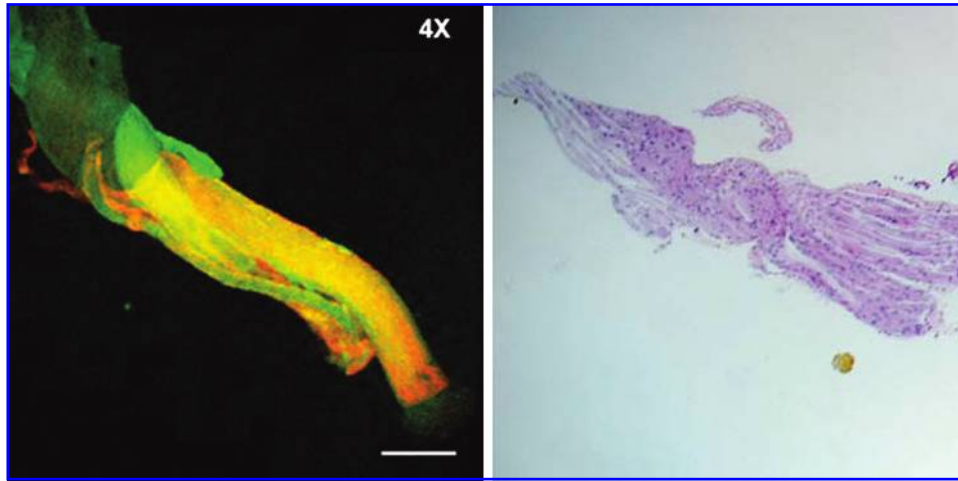


FIG. 4. Low magnification (4×) multiphoton microscopy image of rat cavernous nerve. A single optical section from the middle of the tissue is shown. Second harmonic generation signal is from the fibrocollagenous sheath (red) and autofluorescence (green) is from the nerve. Scale bar: 500 μm .

The imaging was performed using intrinsic fluorescence and scattering properties of the tissues without any exogenous dye or contrast agent. A custom-built MPM, consisting of an Olympus BX61WI upright frame and a modified MRC 1024 scanhead, was used. A femtosecond pulsed titanium/sapphire laser (Mai Tai® from Spectra-Physics, Newport Corp, Mountainview, CA) at 780-nm wavelength was used to excite the tissue; laser power under the objective was modulated via a Pockels cell (Conoptics, Inc, Danbury, CT). Second harmonic generation (SHG) signals were collected at 390 (± 35 nm), and broadband autofluorescence was collected at 380 to 530 nm.

Images were acquired at two magnifications: (1) Low magnification for obtaining overall architectural information (4×, 0.28 NA nonimmersion objective). This allows us to image 3 mm² frames at 6 μm /pixel resolution; (2) high magnification for obtaining detailed cellular and local architectural information (20×, 0.95 NA water-immersion objective), which allows us to image 614 μm^2 frames at 1.2 μm /pixel resolution. Higher digital zooms were used to increase magnification, if necessary. When imaging with the 20× objective, a drop of normal saline was placed on the coverslip to achieve water immersion. All images were obtained as stacks of optical sections up to ~ 400 μm into the

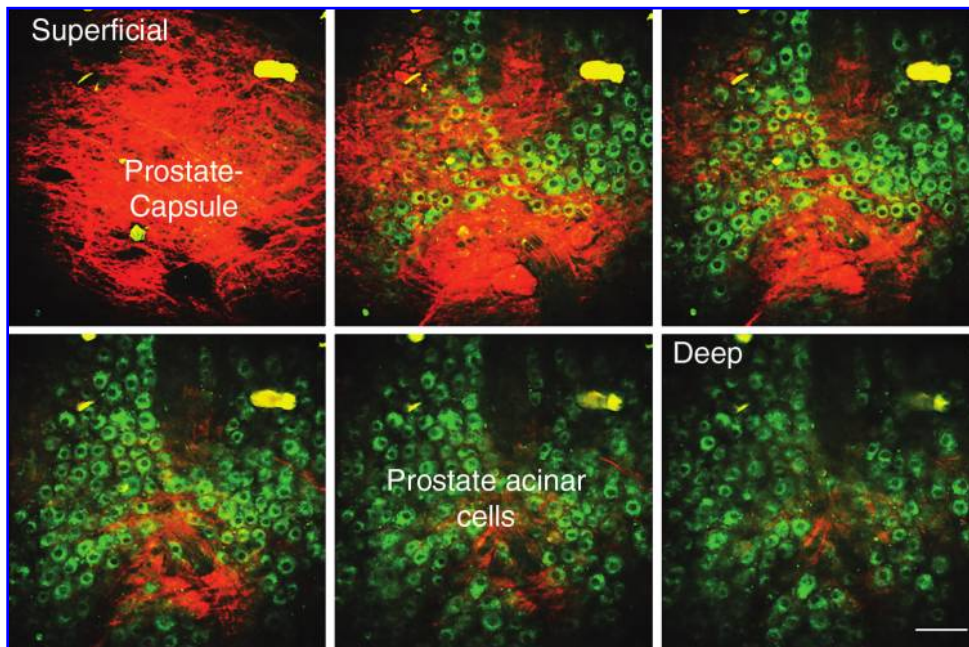


FIG. 5. High magnification (20×) multiphoton microscopy image of another rat prostate specimen, showing several optical sections through the specimen (roughly 10 μm apart). In the superficial optical sections, we see a second harmonic generation (SHG) signal from the fibrous capsule. Deeper sections show prostatic cells (green) and SHG signal from the intervening fibrous stroma (red). Scale bar: 100 μm .

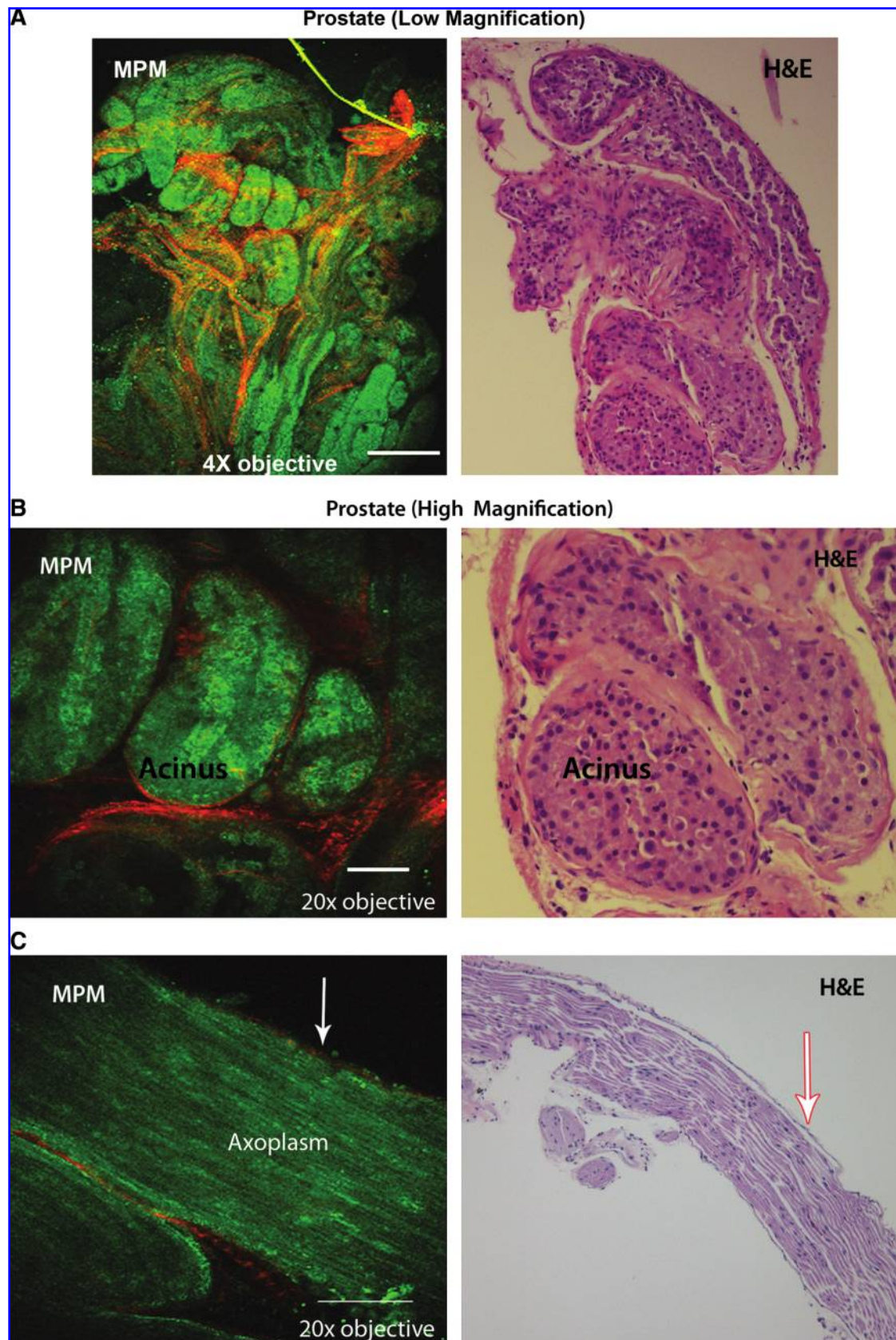


FIG. 6. Multiphoton microscopy (MPM) images and the corresponding hematoxylin and eosin (H&E) stained histologic images for validation of the findings. (A) Prostate lobe at low magnification (4 \times); (B) prostate acini at high magnification (20 \times); (C) cavernous nerve at high magnification (20 \times)—the arrow shows the perineural sheath; (D) major pelvic ganglion (MPG); (E) fat at high magnification (20 \times).

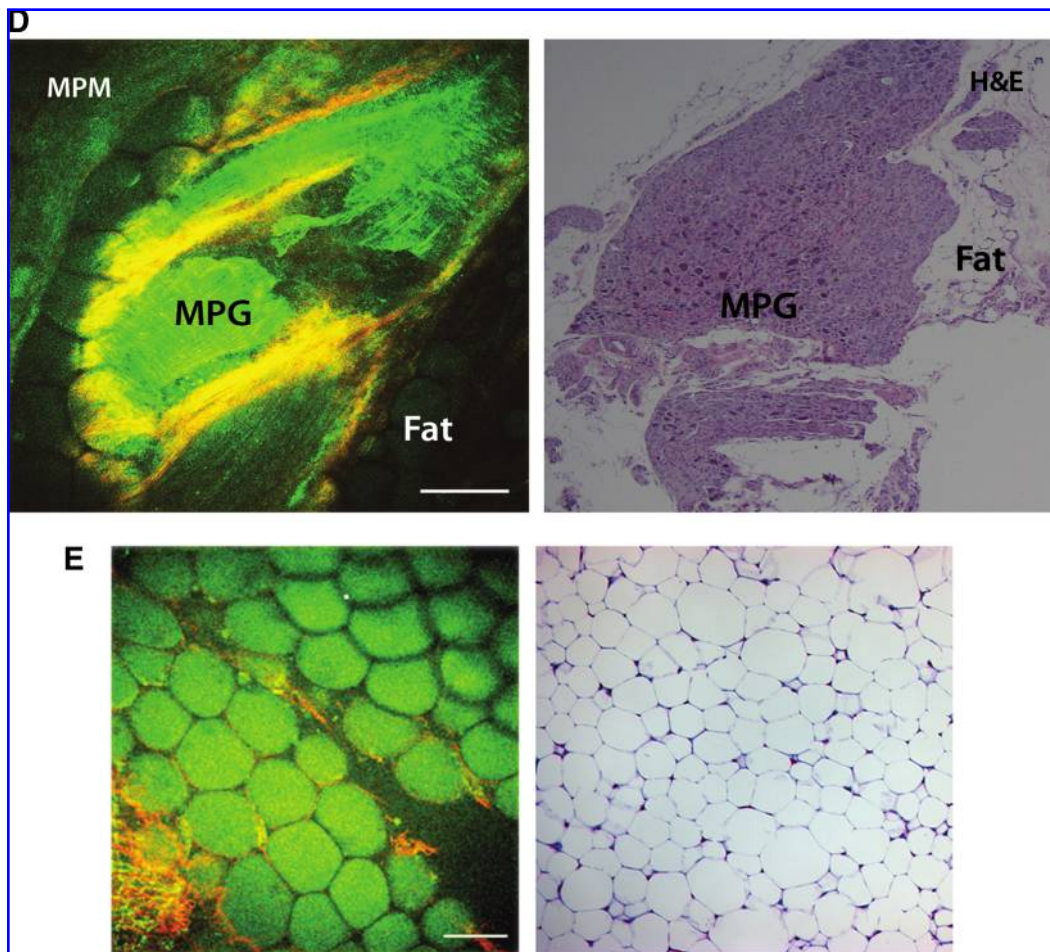


FIG. 6. (Continued)

tissue with the 4 \times objective, and up to $\sim 250 \mu\text{m}$ with the 20 \times objective.

The images obtained from SHG and tissue fluorescence were then merged and color coded during postprocessing for better appreciation of details. The MPM was marked and preserved in 10% formalin and subjected to standard H&E staining for histologic confirmation and correlation.

Results

Using MPM imaging, we were able to obtain images of adequate intensity and resolution to allow correlation with H&E histology. The prostate capsule with underlying acini (Figs. 1 and 2), a large peripheral nerve (Fig. 3), and cavernous nerve (Fig. 4) were carefully dissected and imaged without using any extrinsic labeling agent. A strong SHG signal was observed from the collagen content of the prostate capsule and the periglandular connective tissue in the stroma (Figs. 5 and 6B). Autofluorescence from the cytoplasm defined the boundaries of individual cells that outlined the acini (Figs. 5 and 6B). Similarly, a uniform fluorescence from the axoplasm was the hallmark of nerves (Figs. 3, 4, and 6C).

Varying collagen content (and the resulting SHG signal) of the perineal sheath depending on the size of the nerves—larger from peripheral nerve and smaller from cavernous nerve (compare Figs. 3 and 4)—was observed. Fat was identified by its unique appearance of tilelike polygonal cells and a uniform

fluorescent signal (Fig. 6E). The above described characteristics were observed repeatedly in different experiments.

The ability to image beneath the surface of the tissue in real time is shown in Figure 5. Here, multiple successive optical sections of the prostate were imaged. The information gathered from the stacks of multiple thin optical sections can also be processed in the form of a movie.

Discussion

How can we improve the efficacy of a nerve-sparing procedure during RP without sacrificing any degree of cancer control? We suggest that along with the knowledge of neuroanatomy, “real-time tissue visualization” may help surgeons to localize the nerves and track variations in the course of nerves in proximity to the cancerous tissue. This should minimize nerve damage and also reduce the incidence of residual cancer (positive surgical margins). In this study, we evaluated MPM and the phenomenon of SHG as a technique to improve visualization of nerves in relation to the prostate.

In MPM, a sample is illuminated by near infrared light from a femtosecond pulsed laser. Because tissues are relatively transparent to near infrared light, this light can penetrate relatively deep into the tissue, typically up to $\sim 500 \mu\text{m}$, depending on the absorption and scattering properties of the specific tissue. Multiphoton fluorescence is based on the

simultaneous absorption of two or more low-energy photons by a molecule. While the energy of either of these low-energy photons is insufficient to excite an electron, their combined energy is enough to raise an electron to the excited state and thus stimulate fluorescence. Use of a femtosecond pulsed laser ensures that in the focal volume of the laser, a sufficiently high photon density is achieved for simultaneous absorption of two photons during the Heisenberg uncertainty principle time of $\sim 10^5$ seconds. The excitation of electrons is limited to the focal volume, because the rest of the light path does not have sufficient photon density to achieve a two-photon excitation (2PE).

SHG is another aspect of MPM. It is a nonlinear coherent scattering phenomenon that results from interaction of photons with a noncentrosymmetric material such as collagen. Because of the abundance of collagen in the prostate capsule and prostatic fibromuscular stromal tissue, a clear outline of prostatic glands is seen. Most of the experimental biologic studies that use MPM have used conventional fluorophores (eg, fluorescein) or fluorescent proteins, such as green fluorescent proteins, for labeling and tissue enhancement.¹² A few studies, however, have used 2PE of intrinsic molecules such as nicotinamide adenine dinucleotide phosphate (NAD[P]H)^{13,14} and flavins,¹⁵ three-photon excitation of serotonin,^{16–18} and SHG of collagen, skeletal muscle, and microtubules.^{19–21}

Although the use of extrinsic fluorophore stains can enhance the image quality, there is always a concern about their effect on living tissue. With our aim of investigating an imaging technique that ultimately can be used on live patients during robot-assisted RP, all imaging was performed without any extrinsic dye or contrast agent. Use of a laser light at 740 to 780 nm allowed the excitation of the intrinsic fluorophores present in most living cells (eg, reduced NADH, flavin adenine dinucleotide).

The unique advantage of this technique is the acquisition of high-resolution images without the need for any extrinsic labeling agent. In addition, the use of low energy photons also results in minimal phototoxic effects on living tissue.²² Isolated reports of cavernous nerve imaging after axonal labeling following the injection of nerve tracer in the corpus callosum have been published.²³ The concern for safety of the labeling agent for human tissues and a long retrograde travel time of nerve tracer, however, limit their applicability in the clinic.

Conclusion

Our preliminary experience shows the feasibility of identifying nerves in the periprostatic region in a rat model, along with the ability to image the prostate capsule and underlying cells. Imaging of a rat cavernous nerve was performed in a consistent manner in repeated experiments. Further experience and integration of this imaging technique with the surgical procedure may result in evolution of a better nerve-sparing radical prostatectomy.

Disclosure Statement

Dr. Mukherjee acknowledges support from a K12 award (1 KL2 RR024997-01) from the Clinical and Translational Science Center (CTSC) of the Weill Cornell Medical College.

Dr. Tewari acknowledges support from the Robert P. Lynch Urologic Oncology endowment at Weill Cornell Medical College and Prostate Cancer Foundation Competitive award.

Dr. Webb acknowledges support from an NIH-NIBIB RO1 Bioengineering Research Partnerships (BRP) award (R01-EB006736) from the National Institutes of Health.

References

- Murphy GP, Mettlin C, Menck H, Winchester DP, Davidson AM. National patterns of prostate cancer treatment by radical prostatectomy: Results of a survey by the American College of Surgeons Commission on Cancer. *J Urol* 1994; 152:1817–1819.
- Talcott JA, Rieker P, Propert KJ, Clark JA, Wishnow KI, Loughlin KR, Richie JP, Kantoff PW. Patient-reported impotence and incontinence after nerve-sparing radical prostatectomy. *J Natl Cancer Inst* 1997;89:1117–1123.
- Weldon VE, Tavel FR, Neuwirth H. Continence, potency and morbidity after radical perineal prostatectomy. *J Urol* 1997;158:1470–1475.
- Catalona WJ, Carvalhal GF, Mager DE, Smith DS. Potency, continence and complication rates in 1,870 consecutive radical retropubic prostatectomies. *J Urol* 1999;162:433–438.
- Walsh PC, Marschke P, Ricker D, Burnett AL. Patient-reported urinary continence and sexual function after anatomic radical prostatectomy. *Urology* 2000;55:58–61.
- Walsh PC, Donker PJ. Impotence following radical prostatectomy: Insight into etiology and prevention. *J Urol* 1982; 128:492–497.
- Takenaka A, Murakami G, Soga H, Han SH, Arai Y, Fujisawa M. Anatomical analysis of the neurovascular bundle supplying penile cavernous tissue to ensure a reliable nerve graft after radical prostatectomy. *J Urol* 2004;172: 1032–1035.
- Lunacek A, Schwentner C, Fritsch H, Bartsch G, Strasser H. Anatomical radical retropubic prostatectomy: ‘curtain dissection’ of the neurovascular bundle. *BJU Int* 2005;95:1226–1231.
- Costello AJ, Brooks M, Cole OJ. Anatomical studies of the neurovascular bundle and cavernous nerves. *BJU Int* 2004;94:1071–1076.
- Quinlan DM, Nelson RJ, Partin AW, Mostwin JL, Walsh PC. The rat as a model for the study of penile erection. *J Urol* 1989;141:656–661.
- Sezen SF, Burnett AL. Intracavernosal pressure monitoring in mice: Responses to electrical stimulation of the cavernous nerve and to intracavernosal drug administration. *J Androl* 2000;21:311–315.
- Wang W, Wyckoff JB, Frohlich VC, et al. Single cell behavior in metastatic primary mammary tumors correlated with gene expression patterns revealed by molecular profiling. *Cancer Res* 2002;62:6278–6288.
- Bennett BD, Jetton TL, Ying G, Magnuson MA, Piston DW. Quantitative subcellular imaging of glucose metabolism within intact pancreatic islets. *J Biol Chem* 1996;271:3647–3651.
- Patterson GH, Knobel SM, Arkhammar P, Thastrup O, Piston DW. Separation of the glucose-stimulated cytoplasmic and mitochondrial NAD(P)H responses in pancreatic islet beta cells. *Proc Natl Acad Sci U S A* 2000;97: 5203–5207.
- Xu C, Zipfel W, Shear JB, Williams RM, Webb WW. Multiphoton fluorescence excitation: New spectral windows for

- biological nonlinear microscopy. *Proc Natl Acad Sci U S A* 1996;93:10763–10768.
16. Maiti S, Shear JB, Williams RM, Zipfel WR, Webb WW. Measuring serotonin distribution in live cells with three-photon excitation. *Science* 1997;275:530–532.
17. Williams RM, Shear JB, Zipfel WR, Maiti S, Webb WW. Mucosal mast cell secretion processes imaged using three-photon microscopy of 5-hydroxytryptamine autofluorescence. *Biophys J* 1999;76:1835–1846.
18. Williams RM, Webb WW. Single granule pH cycling in antigen-induced mast cell secretion. *J Cell Sci* 2000;113:3839–3850.
19. Williams RM, Zipfel WR, Webb WW. Multiphoton microscopy in biological research. *Curr Opin Chem Biol* 2001;5:603–608.
20. Campagnola PJ, Millard AC, Terasaki M, Hoppe PE, Malone CJ, Mohler WA. Three-dimensional high-resolution second-harmonic generation imaging of endogenous structural proteins in biological tissues. *Biophys J* 2002;82:493–508.
21. Plotnikov SV, Millard AC, Campagnola PJ, Mohler WA. Characterization of the myosin-based source for second-harmonic generation from muscle sarcomeres. *Biophys J* 2006;90:693–703.
22. Squirrell JM, Wokosin DL, White JG, Bavister BD. Long-term two-photon fluorescence imaging of mammalian embryos without compromising viability. *Nat Biotechnol* 1999;17:763–767.
23. Boyette LB, Reardon MA, Mirelman AJ, Kirkley TD, Lysiak JJ, Tuttle JB, Steers WD. Fiberoptic imaging of cavernous nerves in vivo. *J Urol* 2007;178:2694–2700.

Address reprint requests to:

Ashutosh Tewari, M.D.

Department of Urology

Weill Medical College of Cornell University

Starr 900, 525 East 68th Street

1300 York Avenue

New York, NY 10021

E-mail: akt2002@med.cornell.edu

Abbreviations Used

H&E = hematoxylin and eosin

MPM = multiphoton microscopy

NADH = nicotinamide adenine dinucleotide

RP = radical prostatectomy

SHG = second harmonic generation

2PE = two-photon excitation

MPG = major pelvic ganglion

This article has been cited by:

1. Riccardo Cicchi, Alfonso Crisci, Alessandro Cosci, Gabriella Nesi, Dimitrios Kapsokalyvas, Saverio Giancane, Marco Carini, Francesco S. Pavone. 2010. Time- and Spectral-resolved two-photon imaging of healthy bladder mucosa and carcinoma in situ. *Optics Express* **18**:4, 3840. [[CrossRef](#)]